Physiology-Informed ECG Delineation Based on Peak Prominence

Jonas Emrich, Andrea Gargano, Taulant Koka, Michael Muma

***Abstract*—Reliable wave morphology extraction from the electrocardiogram (ECG) is crucial for enabling effective and trustworthy diagnosis and monitoring of heart conditions. Therefore, we propose a novel physiology-informed ECG delineation algorithm based on prominence information as an explainable metric for morphology point selection. Key advantages are linear runtime complexity, physiology-based parameter choices, and the possibility of enabling real-time waveform annotation within heartbeats in streaming ECG data. Additionally, the proposed method benefits from a multi-lead correction step, enhancing delineation performance when data from multiple leads is available. Evaluations on two ECG databases showcase the superior performance of the proposed prominence delineator compared to established methods. In particular, F_1-scores above 99% are achieved for nearly all morphology waves on the Lobachevsky University Database (LUDB) and QT Database (QTDB), with the only exception of the T-wave on the QTDB. Moreover, standard deviations of detection errors lie significantly below the tolerances set by the Committee of General Standards for Electrocardiography. Our physiology-informed unsupervised signal processing approach therefore concurrently increases performance and explainability compared to the state of the art. An open source implementation is provided to facilitate practitioners to conduct explainable and reliable ECG-based biomarker identification for detecting heart conditions.**

***Index Terms*—ECG, Delineation, Prominence, Waves Detection, Signal Processing**

I. Introduction

The electrocardiogram (ECG) measures the cardiac activity arising from the interplay of several physiological phenomena, primarily involving atrial and ventricular depolarization and repolarization [1]. These phenomena generate prototypical waveforms in the ECG trace, i.e., the P, Q, R, S, and T waves or complexes, whose morphologies (e.g., onsets, offsets, and peaks) characterise the shape of each ECG lead under different physiological and pathological conditions [2] (see Fig. 2). The worldwide clinical application of the ECG as a cost-effective and powerful tool for heart condition monitoring has fostered longstanding collaborative research of physicians and the signal processing community, to improve diagnostic interpretation by devising reliable automatized approaches for ECG waveform delineation [1], [3]. Accordingly, several ECG delineation algorithms have been proposed. In particular, Di Marco et al. [4] devised a delineation method based on the wavelet transform (WT) on a single ECG lead. Similarly, Kalyakulina et al. [5] employed the WT for their custom multi-lead algorithm, whereas Bote et al. [6] proposed a low-complexity algorithm leveraging information about the second derivative of the ECG signal. Recently, Chen et al. [7] conceived a modular multi-lead approach, introducing the local distance transform to determine wave boundaries. Despite the good delineation performances these approaches demonstrate on publicly available databases [7]–[9], a major drawback of current ECG delineation algorithms lies in their explainability. From a physician's perspective, it would be highly desirable to understand all parameters of an algorithm to rule out, e.g., data-driven hyperparameter tuning possibly leading to incorrect heart condition evaluations [3].

This work addresses this issue, by proposing a physiology-informed approach to explainable ECG delineation. Our proposed delineation method builds upon the peak prominence, a geometrically easily interpretable measure of relative height of a peak w.r.t. a baseline, which serves as a decision metric for the selection of fiducial point candidates. The method relies on the accurate identification of appropriate search windows. After segmenting the ECG based on a sample-accurate R-peak detector [10], the search windows are defined by physiologically grounded constraints on the wave durations (cf. Table I). Furthermore, our approach benefits from multiple lead recordings to improve its delineation capabilities. Benchmarking against state-of-the-art methods was performed on multiple ECG databases, not only demonstrating superior power in terms of F_1-score but also fulfilling standard electrocardiographic requirements [1].

Organization: Section II introduces the procedure and complete pipeline of the proposed delineator. Then, numerical results and benchmarks against established methods on public ECG databases are presented in Section III, following a conclusion and outlook into future work in Section IV.

II. Proposed ECG Delineation Method

This section presents the pipeline (Fig. 1) for the proposed delineation method. It begins by preprocessing the ECG signal, followed by an R-peak detection step, segmenting the signal into search regions around the R-peaks for subsequent

Andrea Gargano is with the Dipartimento di Ingegneria dell'Informazione and Research Center "E. Piaggio", Università di Pisa, Pisa, Italy (email: andrea.gargano@phd.unipi.com). His work has been supported by the Italian Ministry of Education and Research (MIUR) in the framework of the ForeLab projects (Departments of Excellence).

Taulant Koka (email: taulant.koka@tu-darmstadt.de) and Michael Muma (email: michael.muma@tu-darmstadt.de) are with the Robust Data Science Group at TU Darmstadt, Germany. Their work has been funded by the ERC Starting Grant ScReeningData under grant number 101042407.

The work of the first author has been funded by the LOEWE initiative (Hesse, Germany) within the emergenCITY center.

The authors thank the BMBF curATime Cluster4Future for valuable inputs.

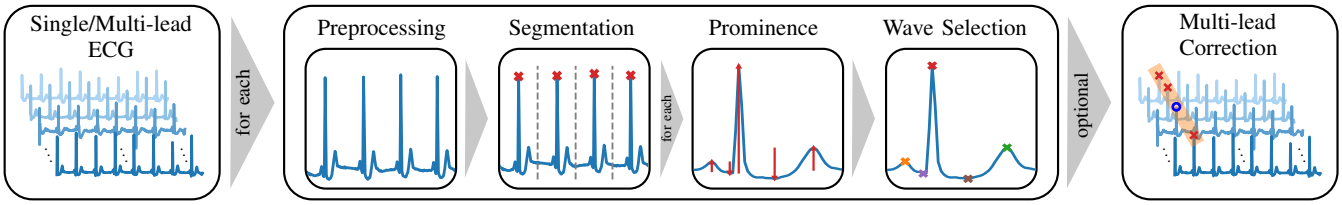

Fig. 1. Pipeline of the proposed ECG delineation approach. A multi-lead correction can be applied in postprocessing, if multiple leads are available.

wave detection (Section II-A). Prominence information (see Section II-B) is then adopted to determine morphology points based on physiology-informed regions (Section II-C). Finally, detections can be further improved in a postprocessing step, if multiple leads are available (Section II-D). The procedure is detailed in the following, and a Python implementation is publicly available on the author's GitHub page [11]. Finally, Section II-E is dedicated to the analysis of the proposed method's computational complexity.

A. R-peak Detection and ECG Segmentation

After reducing slow drifts, DC offset and powerline interference according to the default cleaning in the popular python package *NeuroKit2* [12], the ECG delineation algorithm commences by extracting the R-peak positions as reference points for identifying the P, Q, S, and T wave fiducial points (see Fig. 2). While the R-peak detection can be accomplished by any reliable R-peak detector [12]–[14], in this work, the *FastNVG* [10] was utilized due to its sample-precision and comparably low computation time. Subsequently, the ECG signal is partitioned into disjoint segments centered around the R-peak positions. Therefore, each segment is identified by dividing the signal in the middle between two consecutive heartbeats. These segments serve as regions of interest for the following delineation.

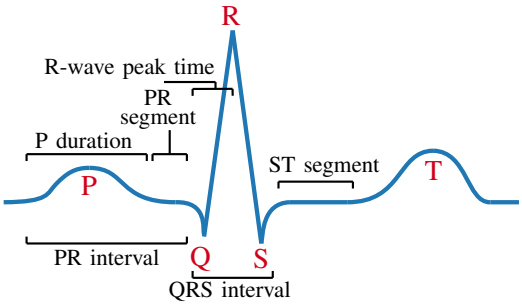

Fig. 2. Schematic representation of P-QRS-T waves in the ECG lead II.

B. Selecting Peak Candidates Using Prominence

For each segment, the prominence is calculated for all local maxima and minima. The peak's prominence is an intuitive measure to distinguish possible peak candidates. It can be understood as the peak's relative height or, in other words, as a measure of how much a peak "stands out" from its surrounding baseline. Let $x_0, \ldots, x_N$ define a discrete signal of length N and let p denote the position of a peak, with associated amplitude x_p. The peak's left and right base points x_{b1} and x_{b2} are found by extending a horizontal line from the peak until it reaches the signal boundaries or a higher peak. Denoting l, r the obtained interval boundaries, the base points are identified as the minimum signal value on each side, i.e., $x_{b1} = \min(x_l, \ldots, x_p)$ and $x_{b2} = \min(x_p, \ldots, x_r)$. Then, the peak prominence is determined as $\mathrm{PP} = x_p - \max(x_{b1}, x_{b2})$. In other words, it is the vertical distance between the peak and the highest base point of its corresponding contour line. This procedure is illustrated with an example in Fig. 3.

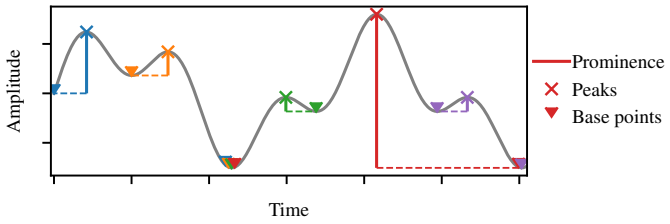

Fig. 3. Illustration of the peak prominence and base points for local maxima.

C. Waves Detection and Delineation

The morphology points are determined within physiologically motivated regions of interest (see Fig. 2) based on prominence information, ultimately leading to an unsupervised approach that is void of any parameter tuning.

Q-waves are detected as the local minima exhibiting the largest (negative) prominence within an interval of 120 ms, given as an upper limit for the R-wave peak time (RWPT), i.e., the duration between the first onset of the QRS complex and the R-peak (see Fig. 2). For normal cases, the RWPT is shorter than 50 ms [15] but it reaches values larger than 100 ms for prolonged cases [16]. Then, the P-wave is selected as the local maximum with the greatest prominence before the Q-wave, constrained not to exceed a PR interval of 300 ms, as typical physiological length is 120−200 ms [2].

Following an R-peak, the S-wave is identified as the first local minimum after the R-peak, within a physiologically motivated search interval provided by the maximum duration of the QRS complex. The QRS duration is typically below 100 ms and is considered as prolonged and abnormal for values surpassing 120 ms [15], [17]. Therefore, S-waves are selected within 180 ms after the corresponding Q-wave, to consider also prolonged morphologies. To take normal and inverted T-waves into account, the T-wave is determined as the local maximum or minimum exhibiting the largest prominence

TABLE I
SEARCH WINDOW BOUNDARIES BASED ON LITERATURE.

P-wave	Q-wave	S-wave	T-wave
$\leq 120\,\mathrm{ms}$ before Q-wave [2]	≤ 120 ms before R-peak [15], [16]	$\leq 180\,\mathrm{ms}$ after Q-wave [15], [17]	$\geq 150\,\mathrm{ms}$ after S-wave until right segment boundary [2]

after the S-wave, setting a minimum distance of the ST segment of $150\,\mathrm{ms}$ [2]. Finally, the onset and offset of waves are determined through the peak's base points directly obtained through prominence calculation, which lie within the segment boundaries. The search window boundaries are summarized in Table I.

D. Combining Multiple Leads

When data from multiple ECG leads is available, further information can be inferred and used to improve the detections, aligning with various methods that make use of multi-lead data [5], [7]. The employed approach conducts a postprocessing step that corrects the wave detections based on results from all available leads. This allows not only to leverage multi-lead information, but also single-lead applications of the algorithm. This procedure follows the approach by [9]: discarding detections found in less than a third of the leads while detections present in at least two thirds of the leads are set for all leads, using their average position. For settings providing only two leads (e.g., [8]), detections from both signals are combined by averaging positions representing the same wave and including detections only found in one lead.

E. Computation and Complexity

The proposed algorithm enables real-time beat annotation by processing R-peaks in streaming data, detecting morphological points for each P-QRS-T complex with a delay of only one beat. Given R-peak locations, the computational complexity of the subsequent wave detection can be characterized as follows. For each segment, the local extrema are obtained through a linear search. Then, the prominence calculation is performed within segments around each R-peak, where the algorithm must search for the base points of each local extremum. The number of extrema depends on the segment length and is bounded by a constant, the maximum interbeat interval, which is determined by physiological boundaries, e.g., $2\,\mathrm{s}$ [18]. Since the number of R-peaks grows proportionally with the length N of the ECG signal and the subsequent decision procedure in search regions consists of linear operations, it follows that the whole delineation procedure (excluding the R-peak detection) exhibits a linear time complexity $\mathcal{O}(N)$.

III. RESULTS

In this section, we report on experiments involving the proposed delineator and established methods on real-world data. The competing methods are either based on the discrete wavelet transform (DWT) [4], [5], [19], [20] or on filtering and derivatives [6], [7]. To the author's knowledge, no publicly available implementations exist for several state-of-the-art delineators. Consequently, this study relies on, and is limited to, the performance results reported by the authors in [4]–[7]. Additionally, the performance of *Neurokit2*'s publicly available delineators based on the DWT [19] as well as peak-detection methods [12] was evaluated for comparison.

A. Evaluation Databases

The evaluation data used in this work consists of publicly available databases including the Lobachevsky University Electrocardiography Database (LUDB) [9] and the QT database (QTDB) [8], covering various cardiovascular diseases along with a broad variety of QRS and ST-T morphologies. The LUDB contains 200 samples of 10 second long 12-lead ECG recordings from healthy volunteers ($N = 143$) and patients collected in a hospital setting. The QTDB is a collection of 105 samples of 15-minute excerpts from several databases (e.g., the MIT-BIH Arrhythmia Database [21] or the European ST-T Database [22]), providing two-channel ECG recordings. Both databases provide peaks, on- and off-sets of P-waves, T-waves and QRS complexes annotated by expert cardiologists.

B. Delineation Performance Evaluation

To ensure a fair comparison against literature data, detections within a $150\,\mathrm{ms}$ long tolerance window around an annotation are considered to be correct, in compliance with the ANSI/AAMI-EC57:1998 standard [23]. If there is a detected point within the tolerance window around an annotation, the detected point is denoted as true positive (TP). Conversely, if no detected point exists inside the tolerance window, a false negative (FN) is counted. If no annotation exists for a corresponding detection, it is labelled as a false positive (FP). Based on this, we computed the sensitivity $\mathrm{Se} = \mathrm{TP}/(\mathrm{TP} + \mathrm{FN})$, positive prediction value $\mathrm{PPV} = \mathrm{TP}/(\mathrm{TP} + \mathrm{FP})$ and F_1-score $\mathrm{F}_1 = 2\mathrm{TP}/(2\mathrm{TP} + \mathrm{FP} + \mathrm{FN})$, where the latter takes precision and recall into account. For all of the three metrics, a higher value is better, with 100% being optimal. In compliance with [4]–[7], [9], [19] the error for each TP detection is computed as the smallest time interval between the detection and the corresponding annotation pooled over all leads. Then, the mean error m across all detections and the average standard deviation σ, obtained by averaging the intra-recording standard deviations, are calculated.

C. Comparison Against Established Methods

Table II shows the results obtained by the proposed method compared to established delineation methods. For both databases, the comparison covers the examination of all leads, considering methods in the literature that either incorporate data from multiple leads [5], [7] or have been assessed to consider multi-lead information [6]. Additionally, our evaluation also includes results obtained using only a single lead to ensure a fair assessment with single-lead algorithms [4], [12], [20].

TABLE II
COMPARISON ON THE LUDB AND QTDB USING A 150 ms TOLERANCE. THE BEST F_1-SCORE FOR EACH WAVE IS HIGHLIGHTED IN BOLD.

				P-onset	P-wave	P-offset	QRS-onset	R-peak	QRS-offset	T-onset	T-wave	T-offset
LUDB	12-lead	Prominence (this work)	F_1(%)	**99.58**	**99.54**	**99.56**	**99.92**	**99.97**	**99.94**	**99.19**	**99.15**	**99.22**
			$m\pm\sigma$(ms)	1.2±4.8	0.6±3.8	0.6±4.0	-0.2±2.0	-0.2±1.8	-6.0±4.0	0.6±6.6	0.2±4.0	2.4±7.6
		Kalyakulina et al. [5][1]	F_1(%)	97.42	97.42	97.42	99.74	-	99.74	-	98.93	98.43
			$m\pm\sigma$(ms)	-2.7±10.0	-0.3±6.2	-0.4±11.4	-8.1±7.7	-	3.8±8.8	-	4.0±7.4	5.7±15.5
		Chen et al. [7][1]	F_1(%)	97.42	97.42	97.42	99.89	99.93	99.89	99.03	99.06	99.03
			$m\pm\sigma$(ms)	2.2±7.4	-0.76±5.5	-6.5±10.7	15.4±14.6	-0.14±3.4	-3.8±13.6	-1.3±8.8	-0.5±5.5	-1.2±6.8
	Single-lead (first)	Prominence (this work)	F_1(%)	**99.75**	**99.82**	**99.82**	**99.81**	**99.81**	**99.81**	**98.30**	**98.33**	**98.54**
			$m\pm\sigma$(ms)	10.6±11.6	2.6±5.8	6.8±9.0	5.8±6.2	1.6±2.0	-9.2±7.2	5.6±16.6	2.6±8.6	14.2±16.0
		NeuroKit Peak [12]	F_1(%)	99.10	99.53	-	-	99.67	-	-	95.84	94.45
			$m\pm\sigma$(ms)	0.4±19.8	3.4±5.2	-	-	1.0±1.8	-	-	8.8±8.4	2.6±21.0
		NeuroKit DWT [12]	F_1(%)	99.25	98.82	98.46	98.30	99.67	96.11	96.61	91.27	87.26
			$m\pm\sigma$(ms)	-3.6±17.4	-12.0±13.6	-11.4±18.6	-40.6±20.4	1.0±1.8	18.4±13.2	15.2±27.8	-8.0±13.6	-11.4±15.4
		ecg-kit [20][2]	F_1(%)	85.25	86.58	87.97	95.27	-	95.26	-	90.03	89.37
			$m\pm\sigma$(ms)	16.2±31.5	12.0±31.1	7.9±22.3	-3.33±14.3	-	3.7±15.9	-	11.9±32.1	-3.4±32.8
QTDB	2-lead	Prominence (this work)	F_1(%)	**99.45**	**99.55**	**99.42**	**99.86**	**99.99**	**99.83**	**96.95**	97.82	**97.46**
			$m\pm\sigma$(ms)	7.4±8.2	1.0±6.2	-4.0±7.4	1.6±4.8	-6.2±2.6	-12.6±4.8	8.2±12.6	2.0±7.8	-2.4±9.4
		Kalyakulina et al. [5][1]	F_1(%)	97.66	97.69	97.73	98.33	-	98.33	-	98.24	95.50
			$m\pm\sigma$(ms)	-3.5±13.8	4.3±10.0	3.4±12.7	-5.1±6.6	-	4.7±9.5	-	7.2±13.0	13.4±18.5
		Bote et al. [6][1]	F_1(%)	94.88	96.22	97.72	99.75	99.75	99.43	-	**98.47**	95.50
			$m\pm\sigma$(ms)	20.2±13.1	11.6±6.5	-0.9±9.1	7.0±4.3	-6±4.6	-4.4±9.1	-	9.3±12.4	-10.9±12.5
	Single-lead (first)	Prominence (this work)	F_1(%)	**99.12**	**99.32**	**99.54**	**99.97**	**99.97**	**99.79**	**94.40**	95.43	95.14
			$m\pm\sigma$(ms)	8.4±8.0	2.4±6.4	-2.4±7.6	2.8±4.4	-4.8±2.0	-11.2±4.8	8.6±12.6	3.6±8.4	-1.0±10.2
		NeuroKit Peak [12]	F_1(%)	95.21	95.93	-	-	99.78	-	-	90.11	91.51
			$m\pm\sigma$(ms)	9.6±8.0	3.8±6.0	-	-	-5.6±1.8	-	-	8.0±7.8	-4.4±12.6
		NeuroKit DWT [12]	F_1(%)	98.36	98.51	98.02	90.72	99.78	87.47	81.61	79.80	79.82
			$m\pm\sigma$(ms)	4.2±10.6	-1.6±8.4	-4.4±11.0	-29.0±10.0	-5.6±1.8	3.4±6.0	-1.8±16.6	-0.4±7.6	-12.4±10.2
		Di Marco et al. [4][1]	F_1(%)	94.44	94.44	94.44	-	-	-	-	**98.73**	**98.75**
			$m\pm\sigma$(ms)	-4.5±13.4	-4.7±9.7	-2.5±13.0	5.1±7.2	-	0.9±8.7	-	-0.3±12.8	1.3±18.6
$2\sigma_{CSE}$(ms)				10.2	-	12.7	6.5	-	11.6	-	-	30.6

[1] Data obtained from the original publication as there was no publicly accessible implementation of this method.
[2] Data taken from Kalyakulina et al. [9].

Notably, the proposed detector performs well in both multi- and single-lead settings, yielding high F_1-scores and low errors, especially when using all leads. However, it is also necessary to satisfy the *Common Standards for Electrocardiography* (CSE) committee's recommendations, i.e., the standard deviation σ of the mean error should be smaller than $2\sigma_{\mathrm{CSE}}$ (reported in the last line of Table II), where σ_{CSE} represents a robust estimate of what can be expected from expert cardiologists [1]. Clearly, the proposed multi-lead method satisfies this requirement in both datasets and for all wave types (see Table II). Moreover, while some methods fail to identify different wave types over varying morphologies, in particular T-waves (cf. Fig. 4), and other methods do not report a detailed summary for all fiducial points, the proposed approach provides reliable detections. Overall, the proposed method performs best on the LUDB and QTDB, however, for T-wave detection on the QTDB, the detector by Di Marco *et al.* [4] is able to provide higher values but with larger errors, and performs significantly worse for the other features.

Remark: It is worth noting that while the QTDB is widely used as a reference for validating ECG delineators, it was already acknowledged that its manual annotations exhibit inconsistencies, with a significant percentage reported as inaccurate in previous studies [24] which limits the reliability and accuracy of comparisons based on the QTDB.

D. Inverted T-wave Detection

Identifying relevant patterns, such as inverted T-waves, is crucial to provide a reliable ECG delineation [3]. Fig. 4 illustrates the detected P, Q, R, S, and T waves of delineators with available implementations and the proposed method. Results are compared against annotations of an arbitrary record from the LUDB, providing inverted T-waves. While the proposed prominence delineator identifies the presence of inverted T-waves the DWT and Peak methods fail to correctly detect them and mislabel them as S-waves instead.

E. Runtime

To assess the computational time of the proposed algorithm, it is compared with the available implementations provided by the *NeuroKit2* package. This comparison is conducted by measuring the runtime for the complete processing pipeline of single lead ECG recordings of 30 min from the MIT-BIH Arrhythmia dataset [21], utilizing a single core of an

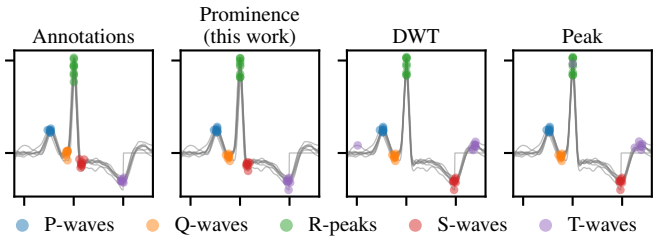

Fig. 4. Comparison of delineated morphology points on LUDB record 7. The inverted T-wave is only detected by the proposed method.

AMD Ryzen 7 1800X processor. For the proposed method, mean computation time $\pm$ standard deviation is given by $2.67 \pm 0.15\,\mathrm{s}$, while the other methods required approximately four times longer. More precisely, the DWT and Peak required $10.26 \pm 1.06\,\mathrm{s}$ and $11.70 \pm 1.80\,\mathrm{s}$, respectively.

IV. Discussion and Conclusion

This work proposes a simple but effective ECG delineation method utilizing physiological and prominence information, allowing the processing of single-lead as well as multi-lead ECG signals. The peak prominence as a decision metric enables higher explainability compared to available approaches [4]–[7] and simultaneously results in a low runtime, exhibiting linear time complexity with signal length. Our benchmark on multiple databases against state-of-the-art methods demonstrates high F_1-scores for all morphology waves. Contrary to previous works, the error standard deviations lie below the requirements of the CSE committee, emphasizing the accuracy of the proposed algorithm. However, since the proposed on- and offset detection strategy is constrained by typical physiological boundaries, strong morphological variations, the presence of impulsive noise and a low SNR level could degrade performance. Developing an approach to robustly identify peak base points might yield further improvements, especially from a clinically relevant perspective [3] and will thus be the subject of future work.

References

[1] "Recommendations for measurement standards in quantitative electrocardiography," *European Heart Journal*, vol. 6, no. 10, pp. 815–825, 10 1985.

[2] R. Northrop, *Non-Invasive Instrumentation and Measurement in Medical Diagnosis*, ser. Biomedical Engineering. CRC Press, 2017, ch. 4.4, pp. 69–77.

[3] J. Schläpfer and H. J. Wellens, "Computer-interpreted electrocardiograms: Benefits and limitations," *Journal of the American College of Cardiology*, vol. 70, no. 9, p. 1183–1192, 2017.

[4] L. Y. Di Marco and L. Chiari, "A wavelet-based ECG delineation algorithm for 32-bit integer online processing," *Biomedical engineering online*, vol. 10, no. 1, pp. 1–19, 2011.

[5] A. I. Kalyakulina, I. I. Yusipov, V. A. Moskalenko, A. V. Nikolskiy, A. A. Kozlov, N. Y. Zolotykh, and M. V. Ivanchenko, "Finding morphology points of electrocardiographic-signal waves using wavelet analysis," *Radiophysics and Quantum Electronics*, vol. 61, no. 8, p. 689–703, Jan. 2019.

[6] J. M. Bote, J. Recas, F. Rincón, D. Atienza, and R. Hermida, "A modular low-complexity ECG delineation algorithm for real-time embedded systems," *IEEE Journal of Biomedical and Health Informatics*, vol. 22, no. 2, pp. 429–441, 2018.

[7] G. Chen, M. Chen, J. Zhang, L. Zhang, and C. Pang, "A crucial wave detection and delineation method for twelve-lead ECG signals," *IEEE Access*, vol. 8, pp. 10 707–10 717, 2020.

[8] P. Laguna, R. G. Mark, A. Goldberg, and G. Moody, "A database for evaluation of algorithms for measurement of QT and other waveform intervals in the ECG," *Computers in Cardiology 1997*, pp. 673–676, 1997.

[9] A. I. Kalyakulina, I. I. Yusipov, V. A. Moskalenko, A. V. Nikolskiy, K. A. Kosonogov, G. V. Osipov, N. Y. Zolotykh, and M. V. Ivanchenko, "LUDB: A new open-access validation tool for electrocardiogram delineation algorithms," *IEEE Access*, vol. 8, p. 186181–186190, 2020.

[10] J. Emrich, T. Koka, S. Wirth, and M. Muma, "Accelerated sample-accurate R-peak detectors based on visibility graphs," in *2023 31st European Signal Processing Conference (EUSIPCO)*, 2023, pp. 1090–1094.

[11] https://github.com/JonasEmrich/prominence-ecg-delineator.

[12] D. Makowski, T. Pham, Z. J. Lau, J. C. Brammer, F. Lespinasse, H. Pham, C. Schölzel, and S. H. A. Chen, "NeuroKit2: A python toolbox for neurophysiological signal processing," *Behavior Research Methods*, vol. 53, no. 4, pp. 1689–1696, feb 2021.

[13] M. Elgendi, M. Jonkman, and F. D. Boer, "Frequency bands effects on QRS detection," in *International Conference on Bio-inspired Systems and Signal Processing*, 2010.

[14] H. Khamis, R. Weiss, Y. Xie, C.-W. Chang, N. H. Lovell, and S. J. Redmond, "QRS detection algorithm for telehealth electrocardiogram recordings," *IEEE Transactions on Biomedical Engineering*, vol. 63, pp. 1377–1388, 2016.

[15] A. R. Pérez-Riera, L. C. de Abreu, R. Barbosa-Barros, K. C. Nikus, and A. Baranchuk, "R-peak time: An electrocardiographic parameter with multiple clinical applications," *Annals of Noninvasive Electrocardiology*, vol. 21, no. 1, pp. 10–19, 2016.

[16] L. F. Pava, P. Perafán, M. Badiel, J. J. Arango, L. Mont, C. A. Morillo, and J. Brugada, "R-wave peak time at DII: A new criterion for differentiating between wide complex QRS tachycardias," *Heart Rhythm*, vol. 7, no. 7, pp. 922–926, 2010.

[17] L. Ilkhanoff, E. Z. Soliman, H. Ning, K. Liu, and D. M. Lloyd-Jones, "Factors associated with development of prolonged QRS duration over 20 years in healthy young adults: The coronary artery risk development in young adults (cardia) study," *Journal of the American College of Cardiology*, vol. 57, no. 14_Supplement, pp. E115–E115, 2011.

[18] T. Yanaga, K. Otsuka, Y. Ichimaru, Y. Hata, K. Okamoto, H. Nakanishi, T. Ueno, M. Yoshioka, M. Nobuyoshi, and M. Ito, "Usefulness of 24-hour recordings of electrocardiogram for the diagnosis and treatment of arrhythmias with special reference to the determination of indication of artificial cardiac pacing." *Japanese circulation journal*, vol. 45 3, pp. 366–75, 1981.

[19] J. Martinez, R. Almeida, S. Olmos, A. Rocha, and P. Laguna, "A wavelet-based ECG delineator: evaluation on standard databases," *IEEE Transactions on Biomedical Engineering*, vol. 51, no. 4, pp. 570–581, 2004.

[20] M. Llamedo, "ecg-kit a matlab toolbox for cardiovascular signal processing," *Journal of Open Research Software*, vol. 4, p. e8, 04 2016.

[21] G. Moody and R. Mark, "The MIT-BIH arrhythmia database on CD-ROM and software for use with it," in *[1990] Proceedings Computers in Cardiology*, 1990, pp. 185–188.

[22] A. Taddei, A. Biagini, G. Distante, M. Emdin, M. Mazzei, P. Pisani, N. Roggero, M. Varanini, R. Mark, G. Moody, L. Braaksma, C. Zeelenberg, and C. Marchesi, "The european ST-T database: development, distribution and use," in *[1990] Proceedings Computers in Cardiology*, 1990, pp. 177–180.

[23] Association for the Advancement of Medical Instrumentation, "Testing and reporting performance results of cardiac rhythm and ST segment measurement algorithms," *ANSI/AAMI EC57:1998/(R2020)*, 2020.

[24] F. González, R. Alcaraz, and J. J. Rieta, "The physionet QT database: Study on the reliability of P-wave manual annotations under noisy recordings," in *2017 Computing in Cardiology (CinC)*, 2017, pp. 1–4.